# Class E compartments form in response to ESCRT dysfunction in yeast due to hyperactivity of the Vps21 Rab GTPase

**Matthew R. G. Russell, Tess Shideler\*, Daniel P. Nickerson\*,‡, Matt West and Greg Odorizzi§**

Department of Molecular, Cellular and Developmental Biology, University of Colorado at Boulder, Campus Box 347, Boulder, CO 80309, USA
‡Present address: Department of Biochemistry, University of Washington, Seattle, WA 98195-7350, USA
*These authors contributed equally to this work
§Author for correspondence (odorizzi@colorado.edu)

## Summary

The endosomal sorting complexes required for transport (ESCRTs) mediate the budding of intralumenal vesicles (ILVs) at late endosomes. ESCRT dysfunction causes drastic changes in endosome morphology, which are manifested in *Saccharomyces cerevisiae* by the formation of aberrant endosomes known as class E compartments. Except for the absence of ILVs, the mechanistic basis for class E compartment biogenesis is unknown. We used electron microscopy to examine endosomal morphology in response to transient ESCRT inactivation and recovery in yeast expressing the temperature-sensitive mutant *vps4ts* allele. Our results show class E compartments accumulate fourfold the amount of membrane normally present at multivesicular bodies and that multivesicular bodies can form directly from class E compartments upon recovery of ESCRT function. We found class E compartment formation requires Vps21, which is orthologous to the Rab5A GTPase in metazoans that promotes fusion of endocytic vesicles with early endosomes and homotypic fusion of early endosomes with one another. We also determined that class E compartments accumulate GTP-bound Vps21 and its effector, the class C core vacuole/endosome tethering (CORVET). Ypt7, the yeast ortholog of Rab7 that in metazoans promotes fusion of late endosomes with lysosomes, also accumulates at class E compartments but without its effector, the homotypic fusion and protein sorting (HOPS), signifying that Ypt7 at class E compartments is dysfunctional. These results suggest that failure to complete Rab5–Rab7 conversion is a consequence of ESCRT dysfunction, which results in Vps21 hyperactivity that drives the class E compartment morphology. Indeed, genetic disruption of Rab conversion without ESCRT dysfunction autonomously drives the class E compartment morphology without blocking ILV budding.

**Key words:** ESCRT, Endosome, Rab

## Introduction

As early endosomes mature into late endosomes, transmembrane proteins targeted for lysosomal degradation are sorted into intralumenal vesicles (ILVs) by the endosomal sorting complexes required for transport (ESCRTs). ILVs are delivered into the hydrolytic interior of the lysosome upon endolysosomal fusion (Piper and Katzmann, 2007). In *Saccharomyces cerevisiae*, ESCRT dysfunction not only blocks ILV budding but also drastically alters endosomal morphology to result in class E compartments (Raymond et al., 1992; Rieder et al., 1996). These aberrant stacks of flattened endosomal cisternae are uniformly observed in yeast in response to ESCRT dysfunction, but the mechanistic basis for their formation has been a mystery. Determining the underlying cause of class E compartment biogenesis might reveal cellular activities not previously known to be functionally linked to ESCRTs.

siRNA-mediated knockdown of most ESCRTs in human cells causes enlarged swollen endosomes, although class E compartments like those in yeast have been observed (Bache et al., 2003; Doyotte et al., 2005; Razi and Futter, 2006). Swollen endosomes are similarly induced upon overexpression of a dominant-active Rab5A GTPase (Stenmark et al., 1994; Wegner et al., 2010). Rab5A regulates early endosomal fusion activity

(Gorvel et al., 1991; Rubino et al., 2000) and is replaced during the course of endosomal maturation by Rab7 (Rink et al., 2005), which regulates fusion of late endosomes with lysosomes (Bucci et al., 2000; Vanlandingham and Ceresa, 2009). Rab5–Rab7 conversion is thought to guide endosomal maturation (Rink et al., 2005; Poteryaev et al., 2010), but its mechanistic basis is poorly understood. In *Caenorhabditis elegans*, Rab conversion requires SAND-1, which promotes endosomal dissociation of the guanonucleotide exchange factor (GEF) that activates Rab5A (Poteryaev et al., 2010). The yeast SAND-1 ortholog, Mon1, is also thought to promote Rab conversion by associating with Ccz1 to form a GEF complex that activates the Rab7 ortholog, Ypt7 (Nordmann et al., 2010).

We show that class E compartments accumulate chronically active Vps21, the yeast Rab5A ortholog, and dysfunctional Ypt7, the yeast Rab7 ortholog. ESCRT dysfunction, therefore, inhibits the completion of Rab5–Rab7 conversion. Hyperactive Vps21 resulting from ESCRT dysfunction causes unregulated endosomal membrane accumulation, which drives the class E compartment morphology. Chronic endosomal localization of Vps9, the GEF that activates Vps21, coupled with impaired endosomal localization of the Mon1–Ccz1 GEF complex that activates Ypt7

(Nordmann et al., 2010), suggests a mechanistic basis for defective Rab conversion in ESCRT-mutant cells. We propose completion of Rab5–Rab7 conversion at endosomes requires ESCRT activity to ensure transmembrane proteins targeted for degradation are sequestered away from the perimeter endosomal membrane before endolysosomal fusion occurs.

## Results

### Membrane accumulation at class E compartments

Vps4 ATPase activity sustains ESCRT function by catalyzing disassembly of ESCRT-III (Wollert et al., 2009). In yeast, prolonged inactivation of a temperature-sensitive mutant $vps4$ allele ($vps4^{ts}$) results in class E compartments (Babst et al., 1997), but intermediate stages of class E compartment formation in $vps4^{ts}$ cells have not been investigated. Therefore, we explored class E compartment biogenesis by electron microscopy (EM) during a time-course analysis of $vps4^{ts}$ cells shifted between permissive (26℃) and non-permissive (38℃) temperatures (Fig. 1A).

Endosomes in $vps4^{ts}$ cells maintained continuously at 26℃ (Fig. 1B) had a normal multivesicular body (MVB) morphology indistinguishable from wild-type yeast (Nickerson et al., 2006). However, the number of ILVs sharply decreased within 10 minutes at 38℃, coincident with a steep rise in non-spherical/flattened endosomes (Fig. 1C; Fig. 2A,B). More extensive endosomal flattening and stacking was observed later,

resulting in a typical class E compartment morphology after 70 minutes of $vps4^{ts}$ inactivation (Fig. 1D,E; Fig. 2B). Within 10 minutes of returning $vps4^{ts}$ cells from 38℃ to 26℃, ILV biogenesis had resumed, and MVBs were abundant after 30 minutes (Fig. 1F,G; Fig. 2C). After 70 minutes, MVBs with normal appearance predominated (Fig. 2C,D; and data not shown). Significantly, ILVs were seen both in stacked cisternae and unstacked flattened endosomes (Fig. 1F,G, white arrowheads). The ILV-containing portions of cisternae were enlarged (Fig. 1F,G, black arrowheads), and cisternae were accompanied by loosely associated MVBs (Fig. 1G), suggesting that many of the MVBs observed during the recovery period derived directly from class E compartments that had formed during $vps4^{ts}$ inactivation. Indeed, class E compartments are probably a source of MVBs for a significant period after $vps4^{ts}$ reactivation because many stacked cisternae and loosely associated endosomes remained at 30 minutes (Fig. 1G; Fig. 2D), with some even observed at 70 minutes (Fig. 1H; Fig. 2D).

We also examined $vps4^{ts}$ cells subjected to a similar temperature-shift protocol by fluorescence microscopy to quantify class E compartment puncta at which the lipid marker, FM 4–64, colocalizes with GFP fused to Sna3, an ILV cargo (Fig. 2F–I). Sna3–GFP is transported from the Golgi to endosomes and subsequently delivered into the lumen of the vacuole (lysosome) in wild-type cells, but it exclusively localizes
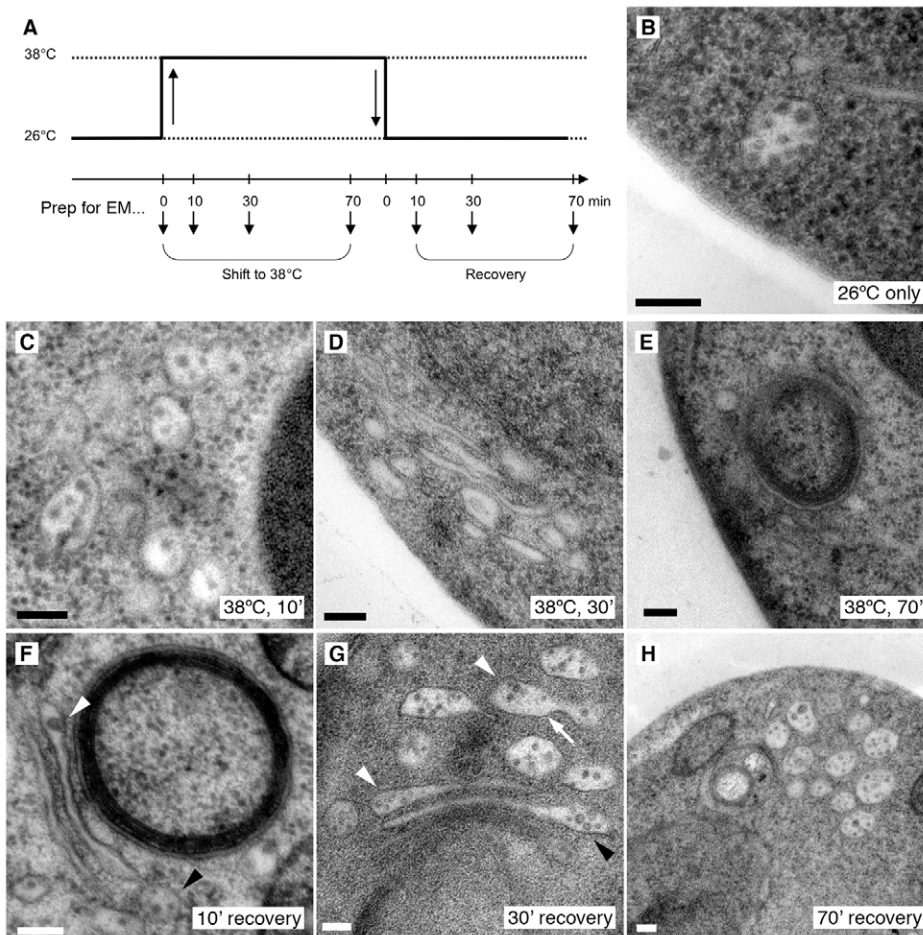


Fig. 1. Formation of class E compartments and restoration of MVBs in temperature-shifted $vps4^{ts}$ cells. (A) Temperature shift protocol. (B–H) Electron micrographs of $vps4^{ts}$ cells that were maintained at 26℃ (B), shifted from 26℃ to 38℃ for the indicated times (C–E), or shifted from 26℃ to 38℃ for 70 minutes and returned to 26℃ for the indicated times (F–H). In F and G white arrowheads indicate ILV budding in flattened stacked class E compartment cisternae and unstacked flattened endosomes; black arrowheads indicate enlarged ILV-containing regions of class E compartment cisternae. In G the dumbbell-shaped MVB profile is indicated by an arrow. Scale bars: 100 nm.
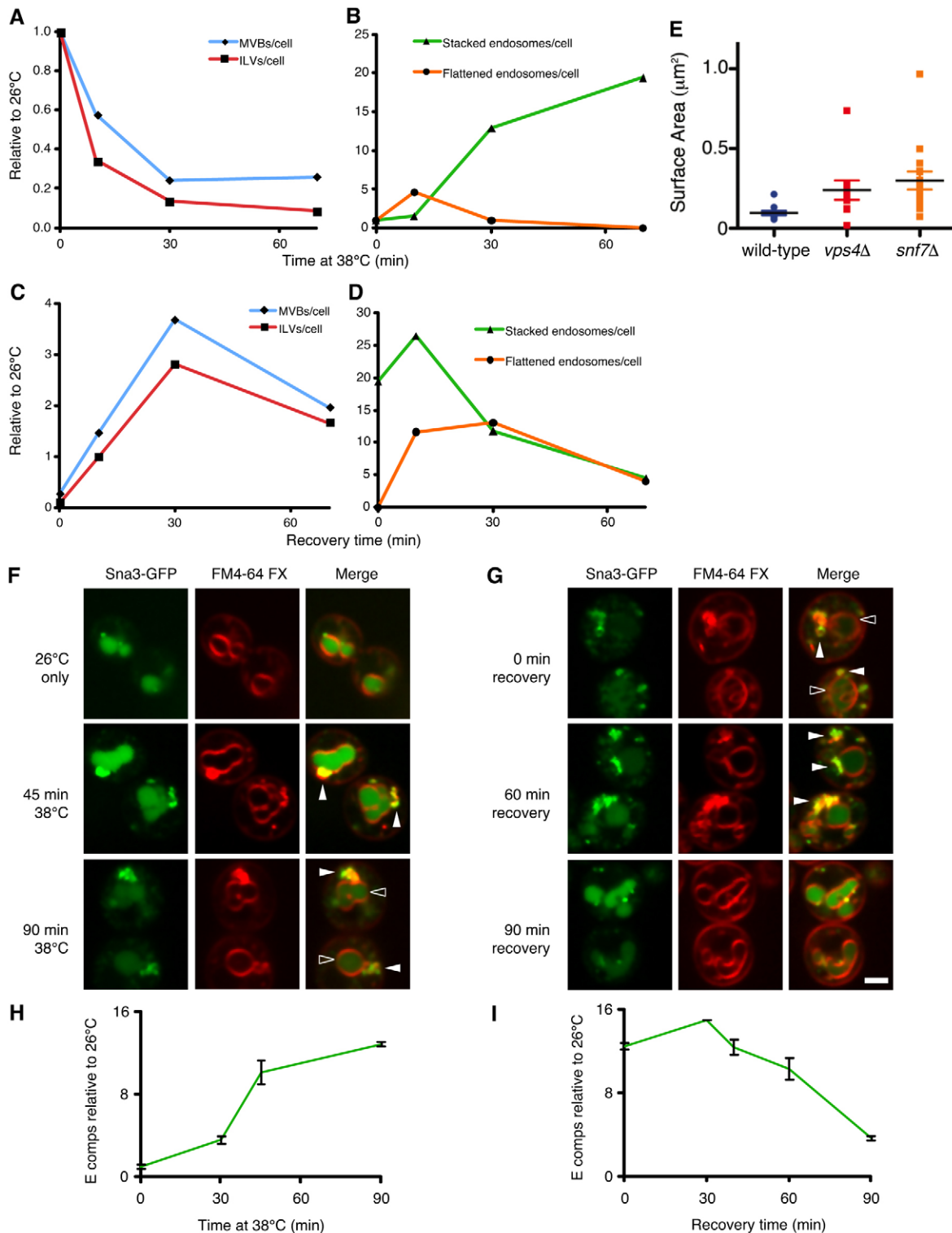
Fig. 2. **Membrane accumulation at class E compartments.** (A–D) Quantification of endosome morphologies in the temperature-shifted *vps4ts* cells from Fig. 1 (frequency relative to *vps4ts* cells maintained at 26°C, $n=50–300$ cell profiles). (E) Mean membrane surface areas of MVBs (including ILVs) relative to individual class E compartment cisternae in electron tomograms of wild-type cells ($0.096\pm0.013$ μm$^2$, $N=11$), *vps4Δ* cells ($0.240\pm0.061$ μm$^2$, $N=10$, $P<0.05$) and *snf7Δ* cells ($0.300\pm0.0561$ μm$^2$, $N=15$, $P<0.01$). (F–I) Quantification of class E compartment biogenesis using confocal fluorescence microscopy. Class E compartments were labeled with FM 4-64FX, a fixable FM 4-64 analog. (F,G) Fluorescence micrographs of Sna3–GFP and FM 4-64FX in temperature-shifted *vps4ts* cells. The indicated times include a 30-minute fixation step. Closed arrowheads, class E compartments marked by both fluorophores; open arrowheads, vacuoles depleted of Sna3–GFP. Scale bar: 2 μm. Images are representative of two independent experiments. (F) Cells shifted to 38°C for the indicated times. (G) Cells shifted to 38°C for 70 minutes and returned to 26°C for the indicated times. (H,I) Quantification of class E compartments marked by both Sna3–GFP and FM 4-64FX in the experiment shown in F and G [mean frequency ($\pm$ s.e.m.) relative to cells maintained at 26°C, $n=140–220$ cells over two independent experiments].

to class E compartments in response to ESCRT dysfunction (Reggiori and Pelham, 2001). The results from this time-course fluorescence analysis support the kinetics of class E compartment formation and recovery of MVB biogenesis that we determined by EM (Fig. 2A–D) and are consistent with previous biochemical analyses showing that endosomal cargoes trapped at class E compartments are delivered to vacuoles after a delay upon reactivation of $vps4^{ts}$ (Babst et al., 1997).

Our EM observation that ILVs and MVBs are formed immediately after reactivation of $vps4^{ts}$ indicates that the resumption in vacuolar cargo delivery is likely due to class E compartments recovering normal endosomal function and morphology prior to late endosome–vacuole fusion rather than direct fusion of class E compartments with vacuoles. Indeed, no structures suggestive of class E compartment–vacuole fusion intermediates were observed by EM after reactivation of $vps4^{ts}$. Surprisingly, 30 minutes of $vps4^{ts}$ recovery yielded a transient threefold increase in the number of ILVs and a fourfold increase in the abundance of MVBs relative to 26℃ (Fig. 2C), suggesting that a significant amount of membrane accumulates at class E compartments. Membrane quantification by electron tomography revealed each class E compartment cisterna in $vps4\Delta$ cells averaged ∼2.5-fold more membrane than the sum of ILVs and perimeter membrane at a typical wild-type MVB (Fig. 2E). Similar results were found in $snf7\Delta$, an ESCRT-III-mutant strain (Fig. 2E). A class E compartment stack typically has three to six cisternae, but ESCRT-mutant cells have fewer class E compartment stacks compared to the number of MVBs in wild-type yeast (Fig. 3F). Nonetheless, class E compartment cisternae in $vps4\Delta$ cells still outnumbered MVBs in wild-type cells by 1.5 fold (0.56 versus 0.36 per cell section, respectively), which, when multiplied by the 2.5-fold membrane excess at each cisterna, indicates the combined membrane content of class E compartments in an ESCRT-mutant cell is ∼4-fold the total membrane represented by all MVBs in a wild-type cell.

### The Vps21 Rab5 GTPase is required for biogenesis of class E compartments but not MVBs

The fourfold membrane excess at class E compartments cannot solely result from the lack of ILVs, which account for only 50% of total MVB membrane (Wemmer et al., 2011). Some accumulation might stem from defective membrane retrieval (Raymond et al., 1992; Piper et al., 1995), but the burst of MVB biogenesis directly from class E compartments upon $vps4^{ts}$ recovery indicated much of the accumulated membrane is en route to vacuoles. Indeed, the amount of excess membrane at class E compartment cisternae (Fig. 2E) implies each can give rise to two or more MVBs, as suggested by the dumbbell-shaped profiles of non-spherical MVBs seen upon $vps4^{ts}$ recovery (Fig. 1G, arrow). Therefore, we investigated if unregulated membrane fusion at endosomes has a role in class E compartment biogenesis.

Membrane fusion is regulated by Rab GTPases, which promote membrane tethering and subsequent assembly of trans-SNARE complexes (reviewed by Stenmark, 2009). In animals, Rab5A promotes fusion of endocytic vesicles with early endosomes and homotypic fusion of early endosomes with one another (Gorvel et al., 1991; Rubino et al., 2000), while Rab7 promotes fusion of late endosomes with lysosomes (Bucci et al., 2000; Vanlandingham and Ceresa, 2009). Among three Rab5 paralogs in yeast, Vps21 is the

functional ortholog of Rab5A (Singer-Krüger et al., 1995), whereas Ypt7 is the only yeast Rab7 ortholog.

The flattened stacks of closely apposed endosomal cisternae characteristic of class E compartments no longer formed upon deletion of $VPS21$ in either $vps4\Delta$ cells (Fig. 3A,E) or in $vps27\Delta$, an ESCRT-0-mutant strain (Fig. 3G,H). Suppression of class E compartment biogenesis was specific to the loss of Vps21 Rab5 activity because class E compartments still occurred in $vps4\Delta$ cells despite deletion of $YPT52$ (Fig. 3I), the only other Rab5 paralog expressed in vegetative yeast (MacKay et al., 2004). Class E compartment biogenesis also was unaffected by deleting $YPT32$ (Fig. 3J), a Rab that regulates endosome-to-Golgi trafficking (Sciorra et al., 2005; Buvelot Frei et al., 2006). Thus, the enlargement of endosomes into flattened, closely apposed cisternae is dependent on Vps21. However, aberrant endosomal morphology remains in ESCRT mutants lacking Vps21 because class E compartments were replaced by loose clusters of abnormal vesicles ∼100 nm in diameter that lacked ILVs (Fig. 3A,H,F).

Although deletion of $VPS21$ suppressed class E compartment formation in $vps4\Delta$ and $vps27\Delta$ cells, it did not restore MVB biogenesis (Fig. 3A,H; see below). Previous studies suggested Vps21 regulates fusion of Golgi-derived transport vesicles with early endosomes (Horazdovsky et al., 1994; Peterson et al., 1999; Tall et al., 1999), and a block in this fusion step could thus indirectly suppress class E compartment formation. However, we still observed MVBs in $vps21\Delta$ cells at low frequency (Fig. 3B,E), suggesting that the loss of Vps21 function either reduced MVB biogenesis or accelerated membrane flux through the late endosome-to-vacuole pathway in some manner. That endosomes remain functional with respect to MVB biogenesis in the absence of Vps21 was further confirmed by our observation that GFP–Cps1 was correctly delivered into the vacuole lumen in $vps21\Delta$ cells. Like Sna3, Cps1 is transported from the Golgi to endosomes where it is sorted into ILVs, but unlike Sna3, Cps1 is mislocalized to both the class E compartments and the vacuole membrane upon ESCRT dysfunction (Odorizzi et al., 1998a). The sorting of GFP–Cps1 in $vps21\Delta$ cells was ESCRT-dependent because it was mislocalized to the vacuole perimeter membrane in $vps21\Delta$ $vps4\Delta$ cells, similar to its vacuolar localization in $vps4\Delta$ cells (Fig. 4). However, in $vps21\Delta$ $vps4\Delta$ cells, GFP–Cps1 no longer colocalized with FM 4-64 at large puncta characteristic of class E compartments (Fig. 4), consistent with loss of the characteristic class E compartment morphology (Fig. 3A,E). $VPS21$ deletion did not cause GFP–Cps1 to bypass endosomes and reach vacuoles directly from the Golgi via the AP3-dependent pathway (Cowles et al., 1997) because deletion of the $APM3$ gene required for AP3 function did not block vacuolar delivery of GFP–Cps1 either in $vps21\Delta$ cells or in $vps21\Delta$ $vps4\Delta$ cells (Fig. 4). Intact vacuoles in these cells support the view that delivery of membrane to this organelle does not absolutely depend on Vps21. However, when $VPS4$ is deleted in addition to $VPS21$, endosomes are unable to support ILV biogenesis even though class E compartments do not form (Fig. 3A).

Unlike deletion of $VPS21$, deletion of $YPT7$ in $vps4\Delta$ cells did not suppress class E compartment biogenesis [Fig. 3C,E; confirmation of class E compartments in this strain by fluorescence microscopy was not possible because of the severe fragmentation of vacuoles caused by $YPT7$ deletion (Wichmann et al., 1992)]. The only obvious difference was that the lumen of class E compartment cisternae in $ypt7\Delta$ $vps4\Delta$ cells
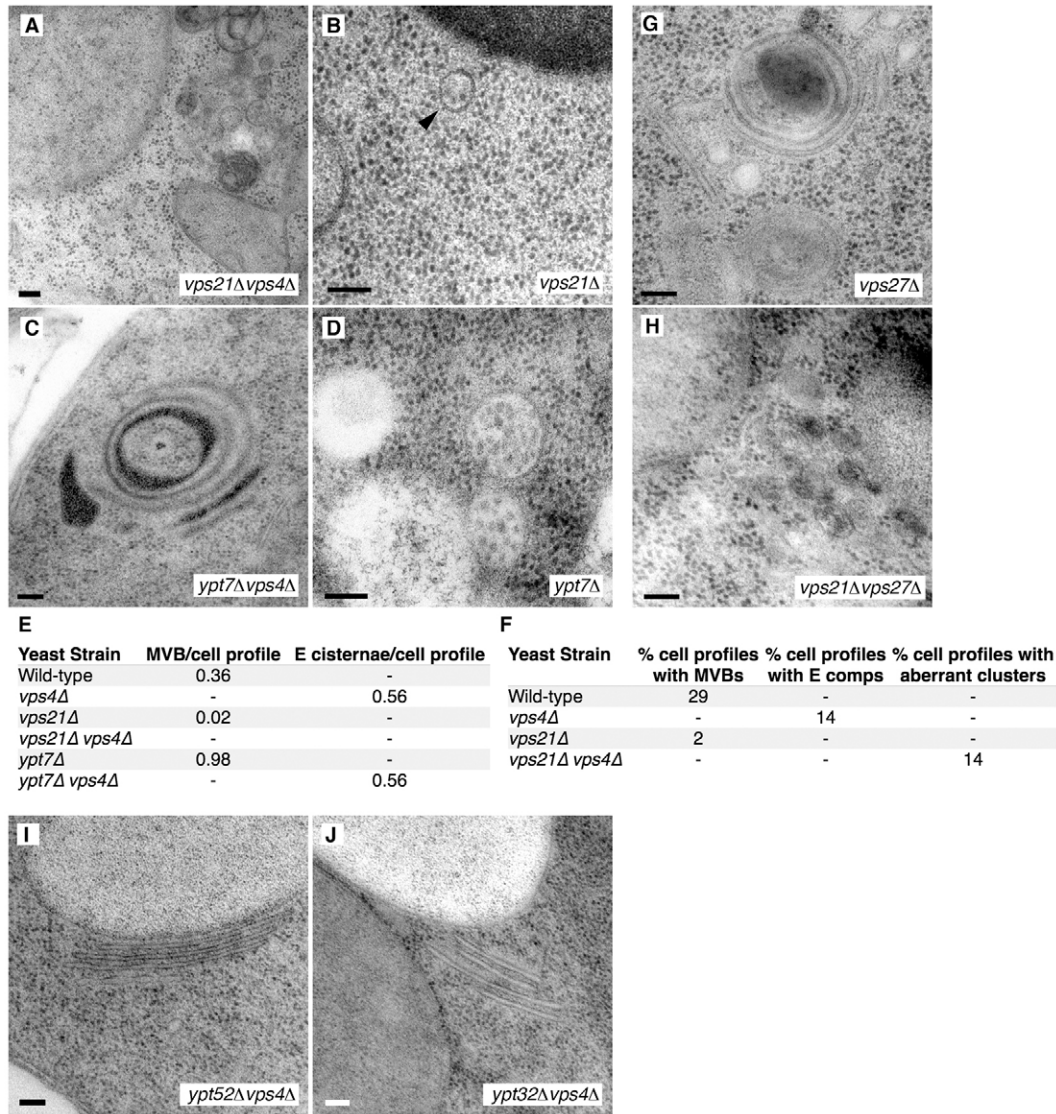
**Fig. 3. Vps21 is required for biogenesis of class E compartments but not MVBs.** (**A–D,G–J**) Electron micrographs of the indicated strains. Scale bars: 100 nm. Arrowhead in B, MVB. (**E**) Quantification of MVBs and class E compartment cisternae represented as frequency of structure per cell profile, $n=50$. (**F**) Quantification of cell profiles containing MVBs, class E compartments, or aberrant vesicle clusters; $n=50$–100.

was occasionally stained more darkly for unknown reasons. Deletion of *YPT7* alone caused a threefold increase in the number of MVBs seen in wild-type yeast (Fig. 3D,E), consistent with Ypt7 mediating late endosome-vacuole fusion. Notably, MVBs in *ypt7Δ* cells were enlarged (mean diameter in wild type=131 nm, *ypt7Δ*=171 nm; $n=40$ for both), suggesting persistent membrane delivery through Vps21 function and/or reduced activity of retromer, which mediates recycling to the Golgi and requires Ypt7 to function (Balderhaar et al., 2010; Liu et al., 2012).

## Vps21 is concentrated at class E compartments in its active GTP-bound state

Because of the requirement for Vps21 but not Ypt7 in class E compartment biogenesis, we compared the localization of GFP–Vps21 versus GFP–Ypt7. As seen previously in wild-type yeast, GFP–Vps21 displayed a punctate distribution, while GFP–Ypt7 localized predominantly to vacuole membranes; however, both

Rabs were concentrated together with FM 4–64 at class E compartments in *vps4Δ* cells (Fig. 5A,B) and in *vps23Δ*, an ESCRT-I-mutant strain (data not shown). In contrast, GFP was not concentrated at class E compartments when fused to Ypt32 (Fig. 5C), the Rab that regulates retrograde transport from endosomes (Sciorra et al., 2005; Buvelot Frei et al., 2006).

We anticipated Vps21 would be concentrated at class E compartments based on its requirement for the formation of these aberrant structures. Although a similar concentration of Ypt7 had been observed previously (Balderhaar et al., 2010), our EM analysis indicated its activity was not required for class E compartment biogenesis (Fig. 3). To evaluate whether the concentration of Vps21 and Ypt7 at class E compartments correlated with each Rab being in the active GTP-bound state, we tested their sensitivity to recombinant GDP dissociation inhibitor (GDI). Upon hydrolyzing their bound GTP, membrane-associated Rabs return to the inactive GDP-bound state. GDI preferentially
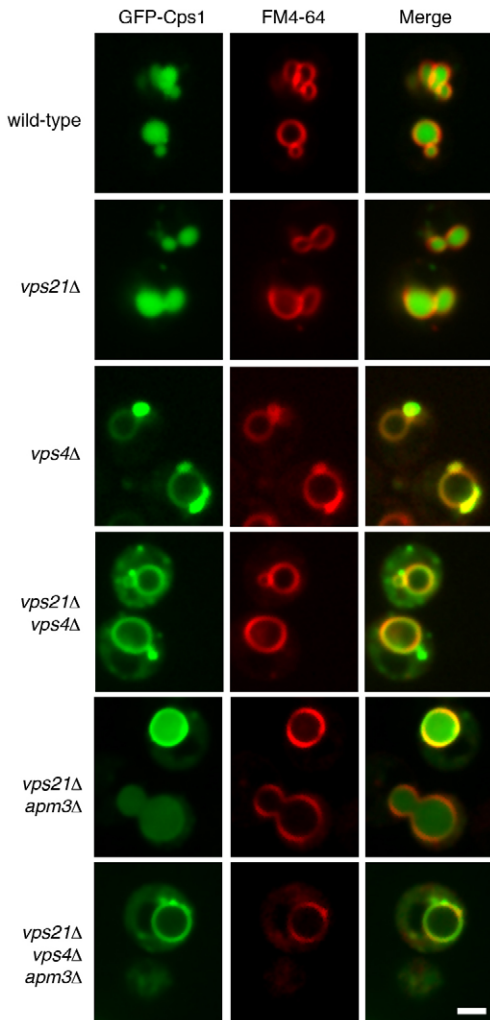
**Fig. 4. Vps21 activity is not required for endosomal membrane trafficking.** Confocal fluorescence micrographs of FM 4-64-stained cells expressing GFP–Cps1. Scale bar: 2 μm.

binds GDP-bound Rabs and extracts them from membranes, solubilizing Rabs and recycling them to the cytosol so that they can engage in subsequent rounds of membrane targeting and function (reviewed by Seabra and Wasmeier, 2004).

Compared to wild-type cells, *vps4Δ* cells contained more membrane-associated Vps21 (Fig. 5D, 12% and 20% of the total fraction recovered in the pellet fraction in wild-type and *vps4Δ* cells, respectively), and membrane-associated Vps21 in *vps4Δ* cells was more resistant to GDI extraction (Fig. 5E, 27% compared to 9% extracted in lanes 2 and 5, respectively). Importantly, the increased GDI resistance of Vps21 in response to *VPS4* deletion was not due to an indirect consequence of the Rab somehow being inaccessible to the addition of recombinant protein because the vast majority of Vps21 could be solubilized by GDI if membranes from *vps4Δ* cells were first incubated with the recombinant catalytic domain of Gyp1 (Gyp1$^{TBC}$), a GTPase-activating protein (GAP) shown *in vitro* to stimulate GTP hydrolysis by both Vps21 and Ypt7 (Albert et al., 1999) (Fig. 5D). The enhanced GDI resistance of Vps21 in *vps4Δ* cells mirrors results recently observed upon disruption of Msb3, a

GAP specific for Vps21 (Nickerson et al., 2012), and signifies that Vps21 is predominantly at class E compartments in its active GTP-bound state upon ESCRT disruption.

Unlike Vps21, the proportion of Ypt7 that was susceptible to extraction by GDI was similar in wild-type and *vps4Δ* cells, even if membranes were first incubated with Gyp1$^{TBC}$ (Fig. 5E, 25% compared to 21% extracted in lanes 2 and 5, respectively). Thus, we did not detect a change in the nucleotide-binding state of Ypt7 upon *VPS4* deletion. However, this assay could not discriminate between Ypt7 localized to class E compartments versus the residual amount detected by fluorescence microscopy at vacuole membranes (Fig. 5B).

## ESCRT disruption inhibits the completion of Rab5–Rab7 conversion

The results described above indicated that Vps21 is concentrated at class E compartments in its active GTP-bound state, but the activation status of Ypt7 concentrated at these aberrant structures was unclear. Therefore, we evaluated the activity of both Rabs by examining the localization of their corresponding effector proteins. Rab effectors bind selectively to active GTP-bound Rabs but not to inactive GDP-bound or nucleotide-free Rabs (reviewed by Stenmark, 2009). Vps21 and Ypt7 have multi-protein effector complexes known, respectively, as the class C core vacuole/endosome tethering (CORVET) (Peplowska et al., 2007) and the homotypic fusion and protein sorting (HOPS) (Seals et al., 2000) complexes. CORVET and HOPS share a common set of four core subunits (the Vps-C proteins: Vps11, Vps16, Vps18 and Vps33) that associate with two additional subunits specific either for Vps21 or Ypt7 (Fig. 6H). Like GFP–Vps21, a CORVET-specific effector, Vps8–GFP (Fig. 6A), was concentrated at class E compartments, as was GFP–Vps33, a core subunit shared by CORVET and HOPS (Fig. 6C). However, GFP–Vps41, a HOPS-specific effector (Fig. 6B), failed to localize to these aberrant structures, signifying that Ypt7 concentrated at this site is nonfunctional. These observations, therefore, suggest that ESCRT dysfunction inhibits the completion of Rab5–Rab7 conversion. Consistent with the suppression of class E compartment morphology by *VPS21* deletion (Fig. 3), Vps8–GFP no longer accumulated in *vps21Δ vps4Δ* cells (Fig. 6I).

Rabs are activated by GEFs, which trigger the release of GDP so that Rabs can bind GTP (Stenmark, 2009). Based on the concentration of GTP-bound Vps21 and CORVET at class E compartments, we anticipated that the Vps21 GEF, Vps9, would similarly be localized at these aberrant structures, where it could drive Vps21 activation. Indeed, Vps9–GFP was aberrantly concentrated at class E compartments in *vps4Δ* cells (Fig. 6D). In contrast, we found that ESCRT dysfunction caused the opposite response for GFP fused to Ccz1, which functions together with Mon1 as the GEF complex that activates Ypt7 (Nordmann et al., 2010). In wild-type yeast, Ccz1–GFP localized to puncta adjacent to vacuoles (Fig. 6E) (Nordmann et al., 2010), but it was not concentrated at class E compartments in *vps4Δ* cells (Fig. 6E). The lack of Ccz1–GFP at class E compartments was not due to defective Mon1–Ccz1 complex formation (Fig. 6F), nor was it due to aberrant proteolytic cleavage of the GFP moiety because western blot analysis of total cell extracts showed no difference in the abundance of Ccz1–GFP between wild-type and *vps4Δ* cells (Fig. 6G). However, Ccz1–GFP exhibited markedly lower expression in wild-type and *vps4Δ*
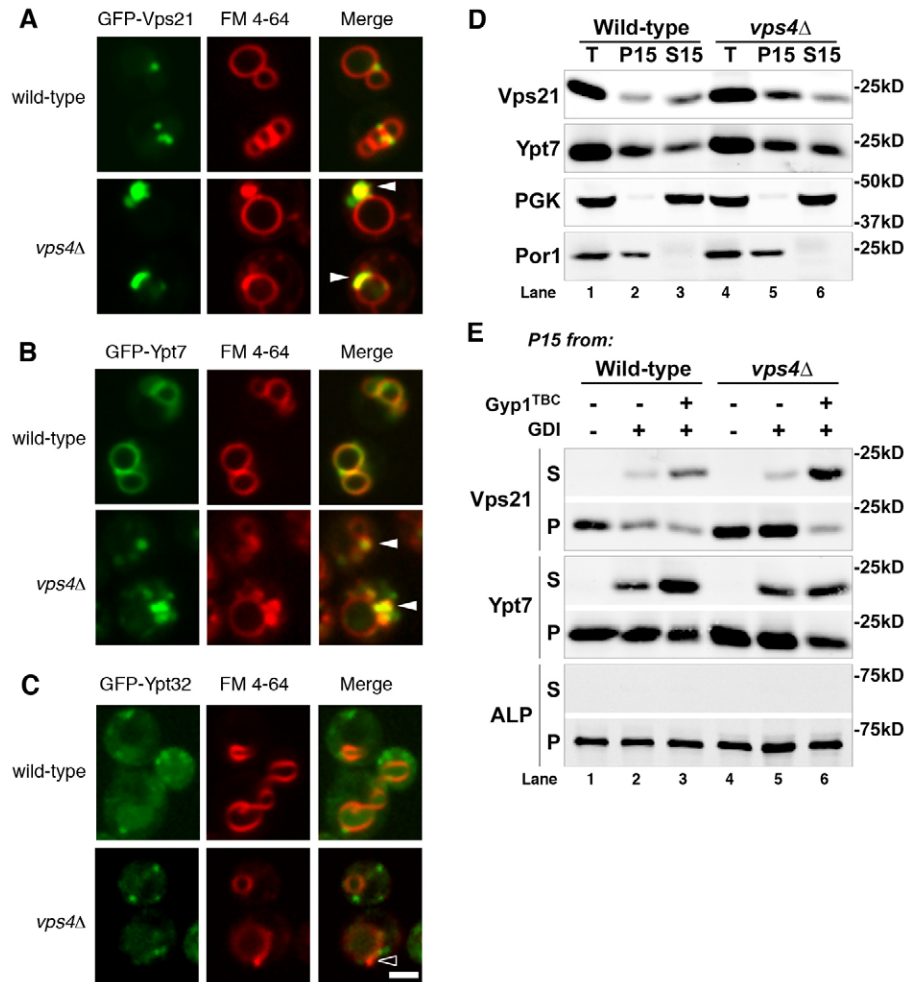
**A**  GFP-Vps21   FM 4-64   Merge
wild-type
vps4Δ

**B**  GFP-Ypt7   FM 4-64   Merge
wild-type
vps4Δ

**C**  GFP-Ypt32   FM 4-64   Merge
wild-type
vps4Δ

**D**
|  | Wild-type | | | vps4Δ | | |
|---|---|---|---|---|---|---|
|  | T | P15 | S15 | T | P15 | S15 |
| Vps21 | | | | | | | -25kD |
| Ypt7 | | | | | | | -25kD |
| PGK | | | | | | | -50kD / -37kD |
| Por1 | | | | | | | -25kD |
| Lane | 1 | 2 | 3 | 4 | 5 | 6 |

**E** *P15 from:*

|  | Wild-type | | | vps4Δ | | |
|---|---|---|---|---|---|---|
| Gyp1^TBC | – | – | + | – | – | + |
| GDI | – | + | + | – | + | + |
| Vps21 S | | | | | | | -25kD |
| Vps21 P | | | | | | | -25kD |
| Ypt7 S | | | | | | | -25kD |
| Ypt7 P | | | | | | | -25kD |
| ALP S | | | | | | | -75kD |
| ALP P | | | | | | | -75kD |
| Lane | 1 | 2 | 3 | 4 | 5 | 6 |

Fig. 5. **Vps21 is concentrated at class E compartments in its active GTP-bound state.** (A–C) Confocal fluorescence micrographs of FM 4-64-stained cells expressing the indicated GFP fusion proteins. Scale bar: 2 μm. Arrowheads, colocalization with FM 4-64-stained class E compartments. (D) Subcellular fractionation of wild-type and vps4Δ cells. PGK1 and mitoporin (Por1) were used as fiducial markers for cytosol and membrane fractions. T, total lysate after 1000 *g* spin; P15, membrane-associated 15,000 *g* pellet fraction; S15, cytosolic 15,000 *g* soluble fraction. (E) Extraction of Rab GTPases Vps21 and Ypt7 by RabGDI. P15 membrane pellets prepared from wild-type or vps4Δ cells were resuspended in lysis buffer or buffer supplemented with 3 μM Gyp1^TBC, and incubated for 15 minutes on ice. Indicated samples received 9 μM recombinant GDI immediately prior to another 15,000 *g* spin in which all samples were again separated to membrane-bound (P) and soluble fractions (S). Alkaline phosphatase (ALP) served as a fiducial marker for sedimentation of membranes.

cells compared to Vps9–GFP (Fig. 6G, expression of each GFP fusion was driven by the endogenous promoters for *CCZ1* and *VPS9*, respectively), which presumably explains why redistribution of Ccz1–GFP elsewhere within vps4Δ cells is not noticeable (Fig. 6E).

## Genetic disruption of Rab conversion can autonomously induce class E compartment biogenesis without ESCRT dysfunction

Having found that class E compartment biogenesis requires Vps21 and that Vps21 is concentrated in its active GTP-bound state along with its CORVET effector at class E compartments, we investigated whether genetically driving chronic Vps21 activity could induce class E compartment biogenesis without mutation of ESCRT genes. The *vps21^{Q66L}* allele encodes a mutant version of Vps21 that has crippled nucleotide hydrolysis activity and is consequently locked in its active GTP-bound state (Tall et al., 1999). However, overexpression of *vps21^{Q66L}* in wild-type yeast resulted in clusters of enlarged MVBs (Fig. 7A) but not class E compartments, suggesting that impaired Ypt7 function might also be required for the formation of class E compartments. Indeed, we found deletion of *YPT7* enabled *vps21^{Q66L}* overexpression to induce flattened, stacked endosomes (Fig. 7B) like those seen during transient inactivation and recovery of *vps4^{ts}* (Fig. 1). The morphological identification of

these class E compartment-like structures as being endosomal in origin was unequivocal because they contained ILVs, and their similarity to bona fide class E compartments in ESCRT-mutant strains was further evident in serial sections, which showed that the stacked endosomal membranes are flattened cisternae, not tubules (Fig. 7B–D). The presence of ILVs in the class E compartment-like structures also demonstrated that ESCRTs are functional in this context with respect to ILV budding. While unbiased quantification showed that class E compartment-like structures were infrequent (Fig. 7E), they were also observed in an independent strain in which the chromosomal *VPS21* locus had been deleted (data not shown). The ability of *vps21^{Q66L}* overexpression in *ypt7Δ* cells to achieve 14% penetrance of the class E compartment phenotype seen upon ESCRT dysfunction (Fig. 7E) (Rieder et al., 1996) must be considered significant because the effects of a functional ESCRT machinery would need to be overcome.

## Discussion

Deletions of ESCRT genes in yeast have long been known to cause the formation of class E compartments (Raymond et al., 1992; Rieder et al., 1996). However, the mechanistic basis for class E compartment biogenesis was unknown. Our results show that the formation of class E compartments is driven by Vps21 hyperactivity coupled with dysfunctional Ypt7 at endosomes.
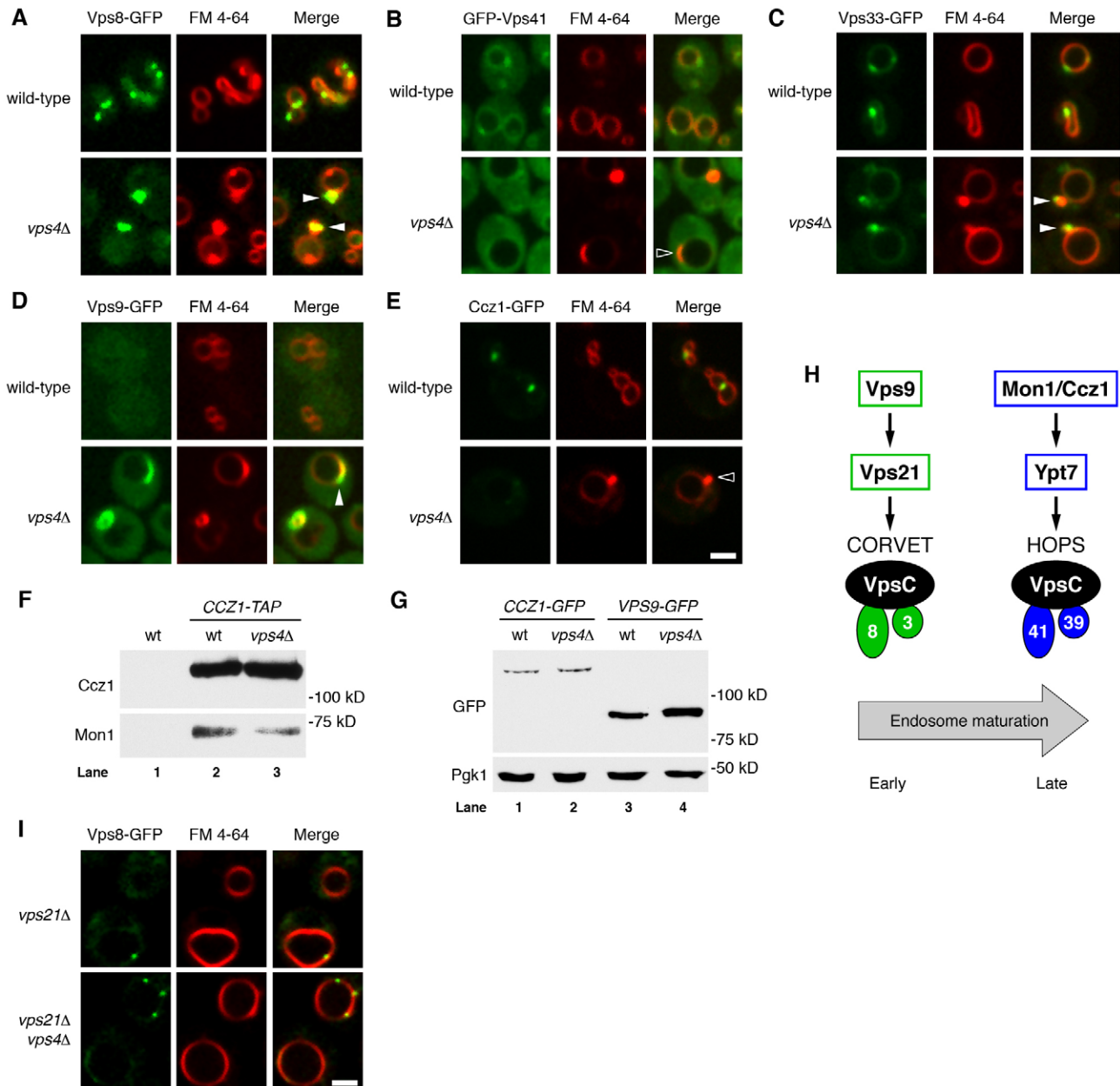
**Fig. 6. ESCRT disruption inhibits the completion of Rab5–Rab7 conversion at endosomes.** (A–E,I) Confocal fluorescence micrographs of FM 4-64-stained cells expressing the indicated GFP fusion proteins. Scale bars: 2 μm. Closed arrowheads, colocalization with FM 4-64-stained class E compartments; open arrowheads, FM 4-64-stained class E compartment without GFP colocalization. In E, identical exposure settings were used for GFP in wild-type and *vps4Δ*. Exposure settings for I were identical to those for A, and strains used for these panels all contained chromosomal integrations of Vps8–GFP controlled by the endogenous *VPS8* promoter. (**F**) Western blot using antibodies against Ccz1 or Mon1 to detect proteins from total lysates that were bound to IgG Sepharose. The *PEP4* gene was deleted in each strain to inactivate vacuolar proteases prior to lysis. (**G**) Western blot analysis of total cell extracts from strains used for D and E. PGK1 was used as loading control. (**H**) Diagram of Vps21 and Ypt7 GEFs and effector complexes.

Vps21 is the yeast ortholog of Rab5A in metazoans (Singer-Krüger et al., 1995), which regulates early endosome fusion events (Gorvel et al., 1991; Bucci et al., 1992; Rubino et al., 2000). Ypt7 is the yeast ortholog of Rab7 in metazoans (Bucci et al., 2000; Vanlandingham and Ceresa, 2009), which replaces Rab5A at endosomal membranes, thereby marking the maturation of early endosomes into late endosomes that can consequently fuse with lysosomes (Rink et al., 2005; Poteryaev et al., 2010). We propose the completion of Rab5–Rab7

conversion requires ESCRT activity to ensure transmembrane proteins targeted for degradation are sequestered away from the perimeter endosomal membrane before endolysosomal fusion occurs.

Chronic Vps21 activity resulting from ESCRT dysfunction was indicated by the aberrant concentration at class E compartments of Vps21 in its active GTP-bound state together with its CORVET effector. Although we could not detect a change in the nucleotide-binding state of Ypt7 in response to
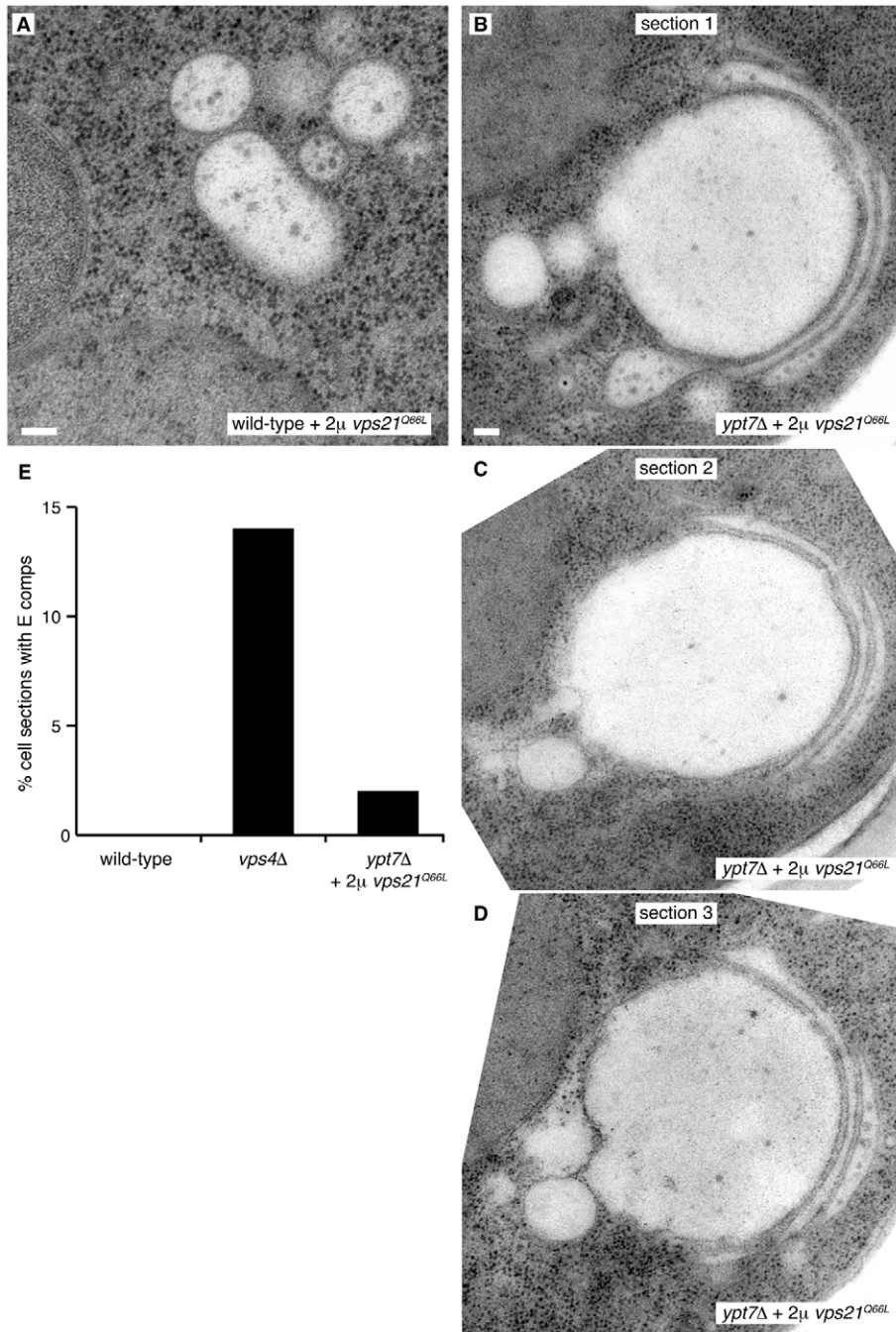
**Fig. 7. Class E compartment biogenesis without ESCRT dysfunction. (A–D)** Electron micrographs of the indicated strains transformed with high-copy (2μ) *vps21^{Q66L}*. (B–D) Consecutive 75-nm serial sections. Scale bars: 100 nm. (**E**) Percentage of cell profiles containing class E compartments; $n = 100$–300 cells.

ESCRT disruption, the absence of its HOPS effector at class E compartments signifies Ypt7 concentrated at these structures was dysfunctional. Vps21 hyperactivity together with the loss of Ypt7 function is a driving force in class E compartment biogenesis because this signature morphological aberration in ESCRT-mutant cells was suppressed by disruption of Vps21 whereas overexpression of dominant-active Vps21 coupled with disruption of Ypt7 induced the class E compartment morphology independently of ESCRT dysfunction. Consistent with our findings are results showing that growth factor stimulation of animal cells activates Rab5A (Barbieri et al., 2000) and enhances the class E compartment morphology caused by ESCRT-I depletion (Razi and Futter, 2006). The relatively low frequency of class E compartment-like structures induced by genetic disruption of Rab conversion in yeast expressing wild-type ESCRT genes (Fig. 7) suggests how challenging it is to form these structures in the context of ESCRT function. The aberrant accumulation of ubiquitin at endosomes, which occurs in response to ESCRT dysfunction (Ren et al., 2008), might also be involved in class E compartment biogenesis because yeast lacking endosomal deubiquitylation activity do not form class E compartments unless cellular ubiquitin levels are maintained (Richter et al., 2007). Evidence that ubiquitylated cargoes inhibit endosomal maturation is the enhanced class E compartment morphology seen upon stimulation of epidermal growth factor receptor endocytosis after ESCRT-I depletion in human cells

(Razi and Futter, 2006). These observations warrant future investigation into whether the ubiquitin-binding capability of Vps9 (Prag et al., 2003), the Vps21 GEF, senses ubiquitylated cargoes accumulated at class E compartments.

The apparent failure to complete Rab5–Rab7 conversion upon ESCRT disruption in yeast correlates with impaired localization of Mon1–Ccz1 at endomembranes. Mon1–Ccz1 is regarded as a key regulator of endosomal Rab conversion (Cabrera and Ungermann, 2010) because the *C. elegans* ortholog of Mon1 inhibits endosomal localization of RABX-5, the GEF that activates Rab5A (Poteryaev et al., 2010). A similar mechanism might exist in yeast because the loss of Ccz1–GFP localization at endosomes coincided with endosomal accumulation of Vps9, the Vps21 GEF (Fig. 6D,E). Because Mon1–Ccz1 also regulates Rab conversion through its function as the Ypt7 GEF (Nordmann et al., 2010), defective endosomal recruitment of Mon1–Ccz1 in ESCRT-mutant cells might account for both Vps21 hyperactivity and the apparent lack of Ypt7 function at class E compartments.

The concentration of Vps9 at class E compartments explains the accompanying accumulation of GTP-bound Vps21 and CORVET, but it is unclear why Ypt7 is also concentrated at class E compartments in the absence of Mon1–Ccz1. That Ypt7 is dysfunctional at these structures without its HOPS effectors is consistent with the severely impaired delivery of endosomal cargoes to vacuoles/lysosomes upon ESCRT disruption (Babst et al., 1997; Doyotte et al., 2005). The accumulation of aberrant vesicle clusters instead of class E compartments in *vps21Δ vps4Δ* cells suggests Ypt7 might also be dysfunctional in this circumstance. While we detected no reduction in GTP-bound Ypt7, impaired Rab7 function in animal cells in response to protein kinase C delta inhibition has similarly been shown to occur without a reduction in GTP-bound Rab7 (Romero Rosales et al., 2009). The mechanistic basis for Ypt7 dysfunction resulting from ESCRT disruption remains to be determined, but it is possible that the persistence of Vps21 and CORVET at endosomes interferes with the ability of Ypt7 to activate HOPS assembly due to CORVET and HOPS sharing a common set of core subunits (Peplowska et al., 2007) (Fig. 6H). Notably, overexpression of the constitutively active GTP-locked *ypt7*$^{Q68L}$ allele was unable to suppress class E compartment formation in *vps4Δ* cells (T.S. and G.O., unpublished results), demonstrating that activation of Ypt7 is insufficient to override the aberrant Vps21 activity that drives class E compartment biogenesis.

Despite the reduction in Ypt7 and HOPS localization at vacuoles upon ESCRT disruption (Fig. 5B; Fig. 6B) (Balderhaar et al., 2010), neither homotypic vacuole fusion nor vacuolar fusion with other types of transport vesicles is impaired (Odorizzi et al., 1998b; Balderhaar et al., 2010). The trace amounts of Ypt7 evident at vacuolar membranes upon ESCRT dysfunction might sustain vacuolar membrane fusion activity. Alternatively, ESCRT dysfunction might suppress the effects of Yck3 protein kinase activity, the loss of which reduces dependence on Ypt7 for vacuole membrane fusion (LaGrassa and Ungermann, 2005; Brett et al., 2008).

Notably, ILV budding was not impaired by *vps21*$^{Q66L}$ overexpression in yeast (Fig. 7B–D) or by overexpression of a similar dominant-active Rab5A in human cells (Wegner et al., 2010). ILV biogenesis was similarly unaffected by disruption of Ypt7/Rab7 function (Fig. 3D) (Vanlandingham and Ceresa, 2009). These observations are consistent with Rab conversion occurring downstream of ESCRT-driven ILV budding. The

biogenesis of MVBs has been proposed to be essential during endosomal maturation so that transmembrane proteins targeted for degradation are sequestered before late endosomes fuse with vacuoles/lysosomes (Mellman, 1996). Indeed, when *vps4*$^{ts}$ function is restored by shifting to the permissive temperature, class E compartments resume ILV budding before fusing with the vacuole (Fig. 1), suggesting that removal of ubiquitylated cargoes by the ESCRT machinery is required for effective activation of the endolysosomal fusion machinery.

Vps21 was originally thought to be essential for membrane trafficking from the Golgi to early endosomes (Cowles et al., 1994; Horazdovsky et al., 1994; Becherer et al., 1996; Burd et al., 1996). However, we found that GFP–Cps1 was delivered to the vacuole lumen via ESCRT-mediated sorting despite Vps21 disruption. Cps1 is a transmembrane protein transported from the Golgi to early endosomes, where it is subsequently sorted by the ESCRT machinery into ILVs (Odorizzi et al., 1998a). Therefore, despite a reduction in both the normal frequency and size of MVBs, endosome biogenesis in the absence of Vps21 remains sufficient for ESCRT-mediated protein sorting into the MVB pathway. This observation indicates that Vps21 is essential for class E compartment formation not because of an *ab initio* requirement in endosome biogenesis but, instead, because Vps21 activity is necessary to provide sufficient delivery of membrane for the accumulation at class E compartment cisternae. Partial redundancy with the Ypt52 Rab5 paralog likely explains the continued biogenesis of endosomes without Vps21 function because simultaneous disruption of both Vps21 and Ypt52 abrogates both MVB cargo sorting and ILV biogenesis (Nickerson et al., 2012). However, we found no evidence to support a role for Ypt52 in the formation of class E compartments, which signifies the specificity of Vps21 in class E compartment biogenesis and suggests the effectors of Vps21 and Ypt52 are not identical.

The timing of class E compartment biogenesis relative to endocytic trafficking was previously unknown because almost all studies had described these abnormal structures at steady state in yeast containing deletions of ESCRT genes. Our results confirm class E compartments and MVBs share a common biogenesis, as indicated by the block in ILV formation coupled with the progressive flattening and stacking of endosomes upon *vps4*$^{ts}$ inactivation, followed by the recovery of ILV budding within flattened endosomal cisternae upon *vps4*$^{ts}$ reactivation. Vps4 is the ATPase that catalyzes disassembly of ESCRT-III, which is the final step executed in the ESCRT pathway and is, therefore, essential for sustaining the activity of this machinery (Wollert et al., 2009). Coupled with the disappearance of class E compartments upon *vps4*$^{ts}$ reactivation, our results indicate these aberrant endosomes are not static dead-end structures, which explains the resumption of vacuolar protein sorting seen upon shifting *vps4*$^{ts}$ cells back to permissive temperature (Fig. 2) (Babst et al., 1997).

Unlike yeast, animal cells do not uniformly respond to ESCRT dysfunction by forming class E compartments but, instead, often form swollen, spherical endosomes lacking ILVs (Doyotte et al., 2005; Razi and Futter, 2006). As in yeast, the disruption in ILV budding alone cannot account for all membrane accumulated at these enlarged endosomes (Razi and Futter, 2006), pointing to their formation being driven by sustained membrane fusion. Whether Rab5A in metazoans, like Vps21 in yeast, drives this membrane accumulation merits investigation.

## Materials and Methods

### Yeast strain and plasmid constructions

The yeast strains and plasmids used in this study are listed in supplementary material Table S1. Standard protocols were used for manipulations of *S. cerevisiae* (Guthrie and Fink, 2002) and for DNA manipulations using *Escherichia coli* (Sambrook and Russell, 2001). Plasmids were confirmed by DNA sequence analysis. Gene deletions and chromosomal integrations in yeast were constructed by homologous recombination using site-specific cassettes amplified by PCR (Longtine et al., 1998; Gueldener et al., 2002) or as follows. JAWY1 was constructed by integration of $vps4^{ts}$ from pMB59 (Babst et al., 1997) and counter-selection using 5-fluoroorotic acid. DNY223 and DNY224 were constructed by genomic integration from pRC680 (Buvelot Frei et al., 2006). DNY242 was constructed by genomic integration from pRS406.NOP1pr-GFP-Vps41 (LaGrassa and Ungermann, 2005).

### Fluorescence microscopy

Yeast were grown to logarithmic phase and stained with either FM 4-64 or its fixable analog, FM 4-64 FX (Invitrogen), using a pulse-chase procedure (Odorizzi et al., 2003). Labeled cells were washed and resuspended in water, then placed on slides for viewing. Cells labeled with FM 4-64 FX were fixed as described in Reggiori and Klionsky (Reggiori and Klionsky, 2006) to preserve class E compartments. Confocal fluorescence microscopy was performed using an inverted fluorescence microscope (TE2000-U; Nikon) equipped with an electron-multiplying charge-coupled device camera (Cascade II; Photometrics) and a Yokogawa spinning disc confocal system (CSU-Xm2; Nikon). Images were taken with a 100× NA 1.4 oil objective, acquired using MetaMorph (version 7.0; MDS Analytical Technologies), and processed using Adobe Photoshop CS2 and CS3 software (Adobe Systems, San Jose, CA).

### Electron microscopy

Yeast were grown to logarithmic phase at 25°C or at the indicated temperatures for $vps4^{ts}$ cells, transferred to aluminum planchettes, and frozen in a Balzers HPM010 high-pressure freezer (Bal-tec AG, Liechtenstein). Planchettes were transferred to vials containing freeze substitution solution (0.1% uranyl acetate, 2% glutaraldehyde in anhydrous acetone). Vials were transferred to a freeze substitution machine (Leica EM AFS/AFS2, Vienna, Austria) at −150°C. Samples were warmed to −80°C over 24 hours, then the cells were removed from the planchettes, transferred to chilled tubes, and the freeze substitution solution replaced. After 48 hours, samples were warmed to −60°C. Over the next 96 hours, samples were washed three times with acetone, then 1:3, 1:1 and 3:1 acetone/Lowicryl HM20 (Polysciences, Warrington, PA), and six times with HM20. The HM20 was UV-polymerized for 12 hours and during warming to 20°C over 48 hours. 75-nm thin sections were post-stained in 2% uranyl acetate for 5 minutes and Reynold's lead citrate for 15 minutes. Thin-section imaging employed a Philips CM10 transmission electron microscope at 80 kV. Images were processed using Adobe Photoshop CS2-3 software (Adobe Systems, San Jose, CA).

### EM quantification criteria

Morphological criteria for quantification (Fig. 2A–D) of the $vps4^{ts}$ cells shown in Fig. 1. MVBs were endosomal profiles less than 300 nm in diameter that contained at least two ILVs with visible membrane bilayers; 'flattened endosomes' were non-spherical unstacked endosome profiles either possessing negative curvature at the limiting membrane or a largest limiting membrane diameter more than twice the smallest diameter; 'stacked endosomes' were individual cisternal profiles that met the criteria for 'flattened endosomes' but were also in a stack of at least two cisternae separated by a ribosome-excluding zone. For ILV quantification, all ILVs were counted regardless of the morphology of the compartment in which they were found. At least 150 cells were counted for each experimental condition, except for the 70-minute 38°C time point or the recovery time points, in which 50 cells were counted. Quantification of MVB profiles and class E compartment cisternal profiles in other strains was the same as for MVBs and 'stacked endosomes' above. 'Aberrant vesicle clusters' were at least three ~100 nm vesicles with heterogeneous content, within 30 nm of each other; at least 50 cell profiles were counted for each strain.

### Electron tomography membrane surface area calculations

Electron tomograms of wild-type, $vps4\Delta$ and $snf7\Delta$ cells used to derive models for surface area measurements were previously generated from single experiments (Nickerson et al., 2010; Nickerson et al., 2006; Wemmer et al., 2011, respectively) by the same operator (M.W.) following a similar protocol. IMOD and 3dmod software from the Boulder 3DEM lab (Kremer et al., 1996) was used for tomogram generation and modeling, respectively. The mean membrane surface area of 11 MVBs (including ILVs) from wild-type cells (five 250-nm sections) was compared to the mean membrane surface area of individual flattened cisternae from three class E compartments from $vps4\Delta$ cells and three class E compartments from $snf7\Delta$ cells (two serial 500-nm tomograms and one single 250-nm tomogram, for

each mutant strain) using Prism (GraphPad, La Jolla, CA). An average of ~65% of the complete structure (MVBs and class E compartments) was measured. The irregular extended three-dimensional shape of class E compartments (Rieder et al., 1996) means that their surface area was more likely to be underestimated than for MVBs.

### Subcellular fractionation and GDI extraction

For subcellular fractionation of yeast lysates, 10 $OD_{600}$ units of logarithmically grown cells were harvested by centrifugation at 500×g, resuspended at 10 $OD_{600}$ units/ml in softening buffer (10 mM DTT, 0.1 M Tris-HCl pH 9.4) and incubated at room temperature for 10 minutes. The cells were then centrifuged again at 500 *g*, resuspended at 5 $OD_{600}$ units/ml in spheroplasting buffer (50 mM HEPES-KOH pH 7.2, yeast nitrogen base, casamino acids, 2% glucose, 1 M sorbitol) and converted to spheroplasts by adding purified lyticase enzyme (Zymolyase 20T; Seikagaku, Tokyo, Japan) and incubating for 30 minutes at 30°C. Spheroplasts were collected by centrifugation at 1000 *g*, resuspended in spheroplasting buffer lacking lyticase, centrifuged again, then lysed by resuspension at 10 $OD_{600}$ units/ ml in ice-cold lysis buffer [20 mM HEPES-KOH pH 7.2, 50 mM potassium acetate, 200 mM sorbitol, 0.1 mM Pefabloc SC, 1 mM PMSF, 0.01 mM chymostatin, 1 µg/mL each of aprotinin, leupeptin and pepstatin, and 1× protease inhibitor cocktail (EDTA-free; Roche)]. Lysates were homogenized with 50 strokes in a dounce homogenizer, cleared of cell debris and nuclear membranes by spinning at 1000 *g* for 5 minutes at 4°C, then centrifuged at 15,000 *g* to yield membrane pellet (P15) and supernatant (S15) fractions. P15 fractions were resuspended in lysis buffer, and proteins were harvested from total, P15 and S15 samples upon the addition of 0.15% (vol/vol) sodium deoxycholate and 10% (vol/vol) trichloroacetic acid. The insoluble material was re-precipitated twice by sonication into ice-cold acetone and centrifugation before being sonicated into Laemmli buffer. 0.2 $OD_{600}$ units of each sample was resolved by SDS-PAGE and examined by western blotting.

Purifications of Gyp1$^{TBC}$ (Lo et al., 2012) and Rab GDI (Starai et al., 2007) have been described. Membrane extraction of Rab GTPases by GDI was performed by resuspending P15 membrane pellets from 2.5 $OD_{600}$ units of cell suspension in 125 µl lysis buffer with or without 3 µM recombinant Gyp1$^{TBC}$. Samples were incubated on ice 15 minutes. Some tubes received 9 µM recombinant GDI immediately prior to spinning at 15,000 *g* for 15 minutes, after which the pellets were resuspended in lysis buffer and proteins from both membrane-associated (P15) and soluble (S15) fractions were processed as described above. 0.2 $OD_{600}$ units of each sample was analyzed by SDS-PAGE and western blotting.

### Total cell extracts and affinity purification

Total yeast extracts were generated from 5 $OD_{600}$ units of logarithmically grown cells that were harvested by centrifugation at 500 *g*, resuspended in 10% (vol/vol) trichloroacetic acid, and incubated 30 minutes on ice. Protein precipitates were isolated by centrifugation at 15,000 *g* for 10 minutes at 4°C, and the insoluble material was re-precipitated twice by sonication into ice-cold acetone and centrifugation before being sonicated into Laemmli buffer. One-half $OD_{600}$ units of extract was resolved by SDS-PAGE and examined by western blotting.

For affinity purification of Ccz1–TAP from total detergent-soluble yeast extracts, 10 $OD_{600}$ units of logarithmically grown cells were converted to spheroplasts and lysed as described above, then rotated at 4°C with 0.5% (vol/vol) Triton X-100 for 10 minutes at 4°C and centrifuged 10 minutes at 15,000 *g* at 4°C to generate a detergent-soluble supernatant that was rotated for 30 minutes at 4°C with IgG Sepharose (GE Healthcare). Bound proteins were harvested by centrifugation at 10,000 *g* at 4°C, followed by three rounds of resuspension of the pelleted beads in lysis buffer followed by centrifugation. Bound proteins were eluted from the beads in Laemmli buffer, and 4 $OD_{600}$ units of sample was examined by SDS-PAGE and western blotting.

### Western blot analysis and antibodies

Western blot analysis was performed by chemiluminescence and film exposure or using an Odyssey fluorescence scanner (LI-COR Biosciences, Lincoln, NE), with the latter used for quantification. Mouse monoclonal anti-PGK (3′-phosphoglycerate kinase), anti-POR1 (mitoporin), and anti-ALP (alkaline phosphatase) antibodies were obtained from Invitrogen (Carlsbad, CA), and mouse monoclonal anti-GFP was obtained from Roche (Indianapolis, IN). Polyclonal anti-Ypt7 antibody was a gift of W. Wickner (Dartmouth College, Hanover, NH). Polyclonal anti-Vps21 antisera was a gift of B. Horazdovsky (Mayo Clinic, Rochester, MN). Polyclonal anti-Ccz1 and anti-Mon1 antisera were a gift of Alex Merz (University of Washington, Seattle, WA).

Supplementary material available online at
http://jcs.biologists.org/lookup/suppl/doi:10.1242/jcs.111310/-/DC1

## References

**Albert, S., Will, E. and Gallwitz, D.** (1999). Identification of the catalytic domains and their functionally critical arginine residues of two yeast GTPase-activating proteins specific for Ypt/Rab transport GTPases. *EMBO J.* **18**, 5216-5225.

**Babst, M., Sato, T. K., Banta, L. M. and Emr, S. D.** (1997). Endosomal transport function in yeast requires a novel AAA-type ATPase, Vps4p. *EMBO J.* **16**, 1820-1831.

**Bache, K. G., Brech, A., Mehlum, A. and Stenmark, H.** (2003). Hrs regulates multivesicular body formation via ESCRT recruitment to endosomes. *J. Cell Biol.* **162**, 435-442.

**Balderhaar, H. J. K., Arlt, H., Ostrowicz, C., Brocker, C., Sundermann, F., Brandt, R., Babst, M. and Ungermann, C.** (2010). The Rab GTPase Ypt7 is linked to retromer-mediated receptor recycling and fusion at the yeast late endosome. *J. Cell Sci.* **123**, 4085-4094.

**Barbieri, M., Roberts, R., Gumusboga, A., Highfield, H., Alvarez-Dominguez, C., Wells, A. and Stahl, P.** (2000). Epidermal growth factor and membrane trafficking. EGF receptor activation of endocytosis requires Rab5a. *J. Cell Biol.* **151**, 539-550.

**Becherer, K. A., Rieder, S. E., Emr, S. D. and Jones, E. W.** (1996). Novel syntaxin homologue, Pep12p, required for the sorting of lumenal hydrolases to the lysosome-like vacuole in yeast. *Mol. Biol. Cell* **7**, 579-594.

**Brett, C. L., Plemel, R. L., Lobingier, B. T., Vignali, M., Fields, S. and Merz, A. J.** (2008). Efficient termination of vacuolar Rab GTPase signaling requires coordinated action by a GAP and a protein kinase. *J. Cell Biol.* **182**, 1141-1151.

**Bucci, C., Parton, R., Mather, I., Stunnenberg, H., Simons, K., Hoflack, B. and Zerial, M.** (1992). The small GTPase rab5 functions as a regulatory factor in the early endocytic pathway. *Cell* **70**, 715-728.

**Bucci, C., Thomsen, P., Nicoziani, P., McCarthy, J. and van Deurs, B.** (2000). Rab7: a key to lysosome biogenesis. *Mol. Biol. Cell* **11**, 467-480.

**Burd, C. G., Mustol, P. A., Schu, P. V. and Emr, S. D.** (1996). A yeast protein related to a mammalian Ras-binding protein, Vps9p, is required for localization of vacuolar proteins. *Mol. Cell. Biol.* **16**, 2369-2377.

**Buvelot Frei, S., Rahl, P. B., Nussbaum, M., Briggs, B. J., Calero, M., Janeczko, S., Regan, A. D., Chen, C. Z., Barral, Y., Whittaker, G. R. et al.** (2006). Bioinformatic and comparative localization of Rab proteins reveals functional insights into the uncharacterized GTPases Ypt10p and Ypt11p. *Mol. Cell. Biol.* **26**, 7299-7317.

**Cabrera, M. and Ungermann, C.** (2010). Guiding endosomal maturation. *Cell* **141**, 404-406.

**Cowles, C. R., Emr, S. D. and Horazdovsky, B. F.** (1994). Mutations in the VPS45 gene, a SEC1 homologue, result in vacuolar protein sorting defects and accumulation of membrane vesicles. *J. Cell Sci.* **107**, 3449-3459.

**Cowles, C. R., Odorizzi, G., Payne, G. S. and Emr, S. D.** (1997). The AP-3 adaptor complex is essential for cargo-selective transport to the yeast vacuole. *Cell* **91**, 109-118.

**Doyotte, A., Russell, M. R. G., Hopkins, C. R. and Woodman, P. G.** (2005). Depletion of TSG101 forms a mammalian "Class E" compartment: a multicisternal early endosome with multiple sorting defects. *J. Cell Sci.* **118**, 3003-3017.

**Gorvel, J. P., Chavrier, P., Zerial, M. and Gruenberg, J.** (1991). rab5 controls early endosome fusion in vitro. *Cell* **64**, 915-925.

**Gueldener, U., Heinisch, J., Koehler, G. J., Voss, D. and Hegemann, J. H.** (2002). A second set of loxP marker cassettes for Cre-mediated multiple gene knockouts in budding yeast. *Nucleic Acids Res.* **30**, e23.

**Guthrie, C. and Fink, G. R.** (2002). *Guide to Yeast Genetics and Molecular and Cell Biology*. San Diego, CA: Academic Press.

**Horazdovsky, B. F., Busch, G. R. and Emr, S. D.** (1994). VPS21 encodes a rab5-like GTP binding protein that is required for the sorting of yeast vacuolar proteins. *EMBO J.* **13**, 1297-1309.

**Katzmann, D. J., Sarkar, S., Chu, T., Audhya, A. and Emr, S. D.** (2004). Multivesicular body sorting: ubiquitin ligase Rsp5 is required for the modification and sorting of carboxypeptidase S. *Mol. Biol. Cell* **15**, 468-480.

**Kremer, J. R., Mastronarde, D. N. and McIntosh, J. R.** (1996). Computer visualization of three-dimensional image data using IMOD. *J. Struct. Biol.* **116**, 71-76.

**LaGrassa, T. J. and Ungermann, C.** (2005). The vacuolar kinase Yck3 maintains organelle fragmentation by regulating the HOPS tethering complex. *J. Cell Biol.* **168**, 401-414.

**Liu, T.-T., Gomez, T. S., Sackey, B. K., Billadeau, D. D. and Burd, C. G.** (2012). Rab GTPase regulation of retromer-mediated cargo export during endosome maturation. *Mol. Biol. Cell* **23**, 2505-2515.

**Lo, S.-Y., Brett, C. L., Plemel, R. L., Vignali, M., Fields, S., Gonen, T. and Merz, A. J.** (2012). Intrinsic tethering activity of endosomal Rab proteins. *Nat. Struct. Mol. Biol.* **19**, 40-47.

**Longtine, M. S., McKenzie, A., 3rd, Demarini, D. J., Shah, N. G., Wach, A., Brachat, A., Philippsen, P. and Pringle, J. R.** (1998). Additional modules for versatile and economical PCR-based gene deletion and modification in Saccharomyces cerevisiae. *Yeast* **14**, 953-961.

**Luhtala, N. and Odorizzi, G.** (2004). Bro1 coordinates deubiquitination in the multivesicular body pathway by recruiting Doa4 to endosomes. *J. Cell Biol.* **166**, 717-729.

**MacKay, V. L., Li, X., Flory, M. R., Turcott, E., Law, G. L., Serikawa, K. A., Xu, X. L., Lee, H., Goodlett, D. R., Aebersold, R. et al.** (2004). Gene expression analyzed by high-resolution state array analysis and quantitative proteomics: response of yeast to mating pheromone. *Mol. Cell. Proteomics* **3**, 478-489.

**Mellman, I.** (1996). Endocytosis and molecular sorting. *Annu. Rev. Cell Dev. Biol.* **12**, 575-625.

**Nickerson, D. P., West, M. and Odorizzi, G.** (2006). Did2 coordinates Vps4-mediated dissociation of ESCRT-III from endosomes. *J. Cell Biol.* **175**, 715-720.

**Nickerson, D. P., West, M., Henry, R. and Odorizzi, G.** (2010). Regulators of Vps4 ATPase activity at endosomes differentially influence the size and rate of formation of intralumenal vesicles. *Mol. Biol. Cell* **21**, 1023-1032.

**Nickerson, D. P., Russell, M. R. G., Lo, S.-Y., Chapin, H. C., Milnes, J. M. and Merz, A. J.** (2012). Termination of isoform-selective Vps21/Rab5 signaling at endolysosomal organelles by Msb3/Gyp3. *Traffic* **13**, 1411-1428.

**Nordmann, M., Cabrera, M., Perz, A., Bröcker, C., Ostrowicz, C., Engelbrecht-Vandré, S. and Ungermann, C.** (2010). The Mon1-Ccz1 complex is the GEF of the late endosomal Rab7 homolog Ypt7. *Curr. Biol.* **20**, 1654-1659.

**Odorizzi, G., Babst, M. and Emr, S. D.** (1998a). Fab1p PtdIns(3)P 5-kinase function essential for protein sorting in the multivesicular body. *Cell* **95**, 847-858.

**Odorizzi, G., Cowles, C. R. and Emr, S. D.** (1998b). The AP-3 complex: a coat of many colours. *Trends Cell Biol.* **8**, 282-288.

**Odorizzi, G., Katzmann, D. J., Babst, M., Audhya, A. and Emr, S. D.** (2003). Bro1 is an endosome-associated protein that functions in the MVB pathway in Saccharomyces cerevisiae. *J. Cell Sci.* **116**, 1893-1903.

**Peplowska, K., Markgraf, D. F., Ostrowicz, C. W., Bange, G. and Ungermann, C.** (2007). The CORVET tethering complex interacts with the yeast Rab5 homolog Vps21 and is involved in endo-lysosomal biogenesis. *Dev. Cell* **12**, 739-750.

**Peterson, M. R., Burd, C. G. and Emr, S. D.** (1999). Vac1p coordinates Rab and phosphatidylinositol 3-kinase signaling in Vps45p-dependent vesicle docking/fusion at the endosome. *Curr. Biol.* **9**, 159-162.

**Piper, R. C. and Katzmann, D. J.** (2007). Biogenesis and function of multivesicular bodies. *Annu. Rev. Cell Dev. Biol.* **23**, 519-547.

**Piper, R. C., Cooper, A. A., Yang, H. and Stevens, T. H.** (1995). VPS27 controls vacuolar and endocytic traffic through a prevacuolar compartment in Saccharomyces cerevisiae. *J. Cell Biol.* **131**, 603-617.

**Poteryaev, D., Datta, S., Ackema, K., Zerial, M. and Spang, A.** (2010). Identification of the switch in early-to-late endosome transition. *Cell* **141**, 497-508.

**Prag, G., Misra, S., Jones, E. A., Ghirlando, R., Davies, B. A., Horazdovsky, B. F. and Hurley, J. H.** (2003). Mechanism of ubiquitin recognition by the CUE domain of Vps9p. *Cell* **113**, 609-620.

**Raymond, C. K., Howald-Stevenson, I., Vater, C. A. and Stevens, T. H.** (1992). Morphological classification of the yeast vacuolar protein sorting mutants: evidence for a prevacuolar compartment in class E vps mutants. *Mol. Biol. Cell* **3**, 1389-1402.

**Razi, M. and Futter, C. E.** (2006). Distinct roles for Tsg101 and Hrs in multivesicular body formation and inward vesiculation. *Mol. Biol. Cell* **17**, 3469-3483.

**Reggiori, F. and Klionsky, D. J.** (2006). Atg9 sorting from mitochondria is impaired in early secretion and VFT-complex mutants in Saccharomyces cerevisiae. *J. Cell Sci.* **119**, 2903-2911.

**Reggiori, F. and Pelham, H. R.** (2001). Sorting of proteins into multivesicular bodies: ubiquitin-dependent and -independent targeting. *EMBO J.* **20**, 5176-5186.

**Ren, J., Pashkova, N., Winistorfer, S. and Piper, R. C.** (2008). DOA1/UFD3 plays a role in sorting ubiquitinated membrane proteins into multivesicular bodies. *J. Biol. Chem.* **283**, 21599-21611.

**Richter, C., West, M. and Odorizzi, G.** (2007). Dual mechanisms specify Doa4-mediated deubiquitination at multivesicular bodies. *EMBO J.* **26**, 2454-2464.

**Rieder, S. E., Banta, L. M., Köhrer, K., McCaffery, J. M. and Emr, S. D.** (1996). Multilamellar endosome-like compartment accumulates in the yeast vps28 vacuolar protein sorting mutant. *Mol. Biol. Cell* **7**, 985-999.

**Rink, J., Ghigo, E., Kalaidzidis, Y. and Zerial, M.** (2005). Rab conversion as a mechanism of progression from early to late endosomes. *Cell* **122**, 735-749.

**Robinson, J. S., Klionsky, D. J., Banta, L. M. and Emr, S. D.** (1988). Protein sorting in Saccharomyces cerevisiae: isolation of mutants defective in the delivery and processing of multiple vacuolar hydrolases. *Mol. Cell. Biol.* **8**, 4936-4948.

**Romero Rosales, K., Peralta, E. R., Guenther, G. G., Wong, S. Y. and Edinger, A. L.** (2009). Rab7 activation by growth factor withdrawal contributes to the induction of apoptosis. *Mol. Biol. Cell* **20**, 2831-2840.

**Rubino, M., Miaczynska, M., Lippé, R. and Zerial, M.** (2000). Selective membrane recruitment of EEA1 suggests a role in directional transport of clathrin-coated vesicles to early endosomes. *J. Biol. Chem.* **275**, 3745-3748.

**Sambrook, J. and Russell, D. W.** (2001). *Molecular Cloning: A Laboratory Manual*. New York, NY: Cold Spring Harbor Laboratory Press.

**Sciorra, V. A., Audhya, A., Parsons, A. B., Segev, N., Boone, C. and Emr, S. D.** (2005). Synthetic genetic array analysis of the PtdIns 4-kinase Pik1p identifies components in a Golgi-specific Ypt31/rab-GTPase signaling pathway. *Mol. Biol. Cell* **16**, 776-793.

**Seabra, M. C. and Wasmeier, C.** (2004). Controlling the location and activation of Rab GTPases. *Curr. Opin. Cell Biol.* **16**, 451-457.

**Seals, D. F., Eitzen, G., Margolis, N., Wickner, W. T. and Price, A.** (2000). A Ypt/ Rab effector complex containing the Sec1 homolog Vps33p is required for homotypic vacuole fusion. *Proc. Natl. Acad. Sci. USA* **97**, 9402-9407.

**Singer-Krüger, B., Stenmark, H. and Zerial, M.** (1995). Yeast Ypt51p and mammalian Rab5: counterparts with similar function in the early endocytic pathway. *J. Cell Sci.* **108**, 3509-3521.

**Starai, V. J., Jun, Y. and Wickner, W.** (2007). Excess vacuolar SNAREs drive lysis and Rab bypass fusion. *Proc. Natl. Acad. Sci. USA* **104**, 13551-13558.

**Stenmark, H.** (2009). Rab GTPases as coordinators of vesicle traffic. *Nat. Rev. Mol. Cell Biol.* **10**, 513-525.

**Stenmark, H., Parton, R. G., Steele-Mortimer, O., Lütcke, A., Gruenberg, J. and Zerial, M.** (1994). Inhibition of rab5 GTPase activity stimulates membrane fusion in endocytosis. *EMBO J.* **13**, 1287-1296.

**Tall, G. G., Hama, H., DeWald, D. B. and Horazdovsky, B. F.** (1999). The phosphatidylinositol 3-phosphate binding protein Vac1p interacts with a Rab GTPase and a Sec1p homologue to facilitate vesicle-mediated vacuolar protein sorting. *Mol. Biol. Cell* **10**, 1873-1889.

**Vanlandingham, P. A. and Ceresa, B. P.** (2009). Rab7 regulates late endocytic trafficking downstream of multivesicular body biogenesis and cargo sequestration. *J. Biol. Chem.* **284**, 12110-12124.

**Wang, C.-W., Stromhaug, P. E., Shima, J. and Klionsky, D. J.** (2002). The Ccz1-Mon1 protein complex is required for the late step of multiple vacuole delivery pathways. *J. Biol. Chem.* **277**, 47917-47927.

**Wegner, C. S., Malerød, L., Pedersen, N. M., Progida, C., Bakke, O., Stenmark, H. and Brech, A.** (2010). Ultrastructural characterization of giant endosomes induced by GTPase-deficient Rab5. *Histochem. Cell Biol.* **133**, 41-55.

**Wemmer, M., Azmi, I., West, M., Davies, B., Katzmann, D. and Odorizzi, G.** (2011). Bro1 binding to Snf7 regulates ESCRT-III membrane scission activity in yeast. *J. Cell Biol.* **192**, 295-306.

**Wichmann, H., Hengst, L. and Gallwitz, D.** (1992). Endocytosis in yeast: evidence for the involvement of a small GTP-binding protein (Ypt7p). *Cell* **71**, 1131-1142.

**Wollert, T., Wunder, C., Lippincott-Schwartz, J. and Hurley, J. H.** (2009). Membrane scission by the ESCRT-III complex. *Nature* **458**, 172-177.

**Wurmser, A. E. and Emr, S. D.** (1998). Phosphoinositide signaling and turnover: PtdIns(3)P, a regulator of membrane traffic, is transported to the vacuole and degraded by a process that requires lumenal vacuolar hydrolase activities. *EMBO J.* **17**, 4930-4942.